Optimal GNSS Pulse Blanking in the Presence of Signal Quantization

Daniele Borio[1] *Member, IEEE* and Eduardo Cano[2] *Member, IEEE*

Abstract

Pulsed interference can severely degrade the performance of a Global Navigation Satellite System (GNSS) receiver. For this reason, several mitigation techniques have been developed for reducing the impact of disturbing signals. Among the different pulsed interference mitigation techniques, Pulse Blanking (PB) has received particular attention due to its simplicity and effectiveness. In this paper, the performance of PB is assessed in the presence of signal conditioning and the impact of front-end parameters, such as the number of bits used for quantization and the gain of the Automatic Gain Control (AGC), is analyzed. The theoretical analysis is supported by Monte Carlo simulations and experimental results, which show that signal conditioning plays a fundamental role in the design of interference mitigation techniques.

Index Terms

Pulse Blanking, Global Navigation Satellite Systems, GNSS, Pseudolites, Pulse Interference

I. Introduction

In the last decade, the impact of pulsed interference and its mitigation have been the focus of intense research activities [1]–[4]. Such interest is justified by the allocation of the L5/E5 band for Global Navigation Satellite System (GNSS) transmission and the proposed use of pulsed pseudolite signals. In the L5/E5 band, Distance Measuring Equipment (DME) signals are used for landing applications whereas it has been proposed that, for compatibility reasons, some pseudolites could broadcast in the GNSS bands. Both signals are forms of pulsed interference.

1) Institute for the Protection and Security of Citizen (IPSC), Joint Research Centre, Ispra (VA), Italy. 2) Engineering ingegneria informatica S.P.A., Ispra (VA), Italy Email: daniele.borio@ieee.org, eduardo.cano-pons@ext.jrc.ec.europa.eu

According to [5], a pulsed interfering signal is a form of band-limited noise that is pulsed on and off, usually in a periodic manner. It is noted that there exist several types of interfering signals [5], [6]. Different countermeasures, specific to the different types of interference, have also been developed. The prime focus of this paper is assessing the impact of pulsed interference and Pulse Blanking (PB), which is a technique widely used to mitigate the impact of this form of interference [7], [8]. PB consists of zeroing the received signal samples corrupted by an interference component. A thorough analysis of other forms of interference and mitigation techniques is beyond the scope of this paper.

The L5 modulation will be broadcast in an Aeronautical Radio Navigation Service (ARNS) band and will coexist with other services which transmit pulsed signals. These services include DME, Tactical Air Navigation (TACAN) and Joint Tactical Information Distribution System (JTIDS) [9]. Several studies [1], [9]–[11] have addressed the coexistence between GNSS and ARNS services. In [1], a preliminary analysis on PB is provided. It is shown that PB is a near-optimal technique for the mitigation of strong pulses. Its implementation simplicity and its relatively good performance make it preferable to more complex mitigation techniques such as Interference Cancellation (IC) [3] and Transformed Domain (TD) excision [4], [12]. In [1], two loss models, developed for quantifying the residual Signal-to-Noise Ratio (SNR) degradation caused by PB, are considered. The first model considers the sole excision loss whereas the second introduces a correction term which accounts for residual interference components. The theory developed however neglects the effect of Automatic Gain Control (AGC) scaling and quantization. Although [1] recognizes the importance of a careful AGC and Analog-to-Digital Converter (ADC) design, no results are provided on the interaction between the receiver front-end and the pulse blanker. The analysis developed by [1] was extended by [2] and [9], which experimentally validated the excision loss model. Note that all the results in [2] and [9] were obtained using at least 8 bits for signal quantization. In this case, the impact of the ADC can be effectively neglected. The SNR loss model has been further extended by [10], [11], [13] which considered the case of multiple pulses generated by different sources. The model accounts for possible pulse overlapping. Also in this case, the impact of quantization and AGC scaling is neglected.

A second example of pulsed interference is represented by pulsed pseudolite signals. Pseudolites are ground based transmitters that play the role of GNSS satellites when GNSS signals

are not available. The signals transmitted by pseudolites can easily overpower the much weaker GNSS signals and several techniques have been developed for reducing coexistence problems [14]. These techniques include frequency diversity [15], [16] and signal pulsing. In this paper, signal pulsing in considered. The analysis of the different techniques adopted for reducing interference problems between GNSS and pseudolite signals is beyond the scope of this paper and the interested reader is referred to [14] for a review of the subject.

The impact of pulsed interference on non-participating GNSS receivers, i.e., receivers not implementing any form of mitigation, has been intensively studied [17]–[19] and several models have been developed to predict receiver losses. However, the impact of PB was not considered. A SNR loss model is used in [7] to determine the impact of pulsed pseudolite signals. Also in this case, the excision loss model discussed above and better analyzed in Section IV is found. The analysis in [7] has been conducted by neglecting the impact of quantization and signal conditioning. Previous literature assumes that interference and useful signals are represented by using an infinite number of bits. Even the most recent results [20] on PB neglected quantization effects and experimental results are also provided using ADCs with at least 8 bits [2], [3]. This is a strong assumption since most of the current GNSS receivers operate with a limited number of bits (1 to 3 bits).

In this paper, PB is analyzed and characterized by accounting for signal conditioning. PB is characterized theoretically and by simulations taking into account the effect of quantization and AGC scaling. A theoretical model is developed for quantifying the residual SNR loss obtained after applying PB. The model accounts for the number of bits used for quantization and the AGC gain. The theory developed is then used for the selection of the optimum parameters that minimize the residual PB loss. This analysis is new and extends previous results [1], [7], [10], [20] which neglected the impact of signal conditioning. In addition to this, useful criteria are provided for the design and implementation of PB on GNSS receivers with a limited number of ADC bits. The results obtained are general and can be applied to the different types of pulsed interference.

Furthermore, a Universal Software Radio Peripheral 2 (USRP2) is used to implement a pseudolite transmitting pulsed signals in the L1 band. Experiments conducted in an anechoic chamber have been used to support the validity of the developed theory. The signals broadcast by a Spirent GSS8000 hardware simulator and the USRP2 pseudolite have been collected using

a National Instruments (NI) vector signal analyzer and re-quantization has been implemented to vary the number of bits and change the AGC gain. The data collected have been processed using a GNSS software receiver implementing PB. A robust [21] noise floor estimator has been adopted to determine the variance of the input noise without being significantly biased by the presence of interference pulses. The estimated variance is used to drive the AGC and properly scale the input samples. Experimental results show the benefits of the developed theory, which provides insight into the role of signal conditioning and its impact on PB.

This paper is an extension of the work presented in [22]. More specifically, [22] provided a comparison between IC and PB in the presence of signal conditioning: all the results relative to PB were provided without proof and no experimental analysis was conducted.

The remainder of this paper is organized as follows. In Section II, the signal and system models adopted in the paper are briefly described. Specific emphasis is devoted to signal conditioning and quantization. In Section III, PB is described and its optimality, under specific operating conditions, is discussed. Theoretical results relative to the expected signal loss are presented in Section IV. Simulation and experimental results supporting the validity of the theoretical findings are shown in Section V. Finally, conclusions are provided in Section VI.

II. Signal and System Model

The signal at the input of a GNSS receiver in a one-path additive Gaussian channel and in the presence of pulsed interference can be modeled as

$$r(t) = \sum_{l=0}^{L-1} y_l(t) + i(t) + \eta(t), \tag{1}$$

which is the sum of L useful signals transmitted by L different satellites, a pulsed interfering signal, $i(t)$, and a noise term, $\eta(t)$. Each useful signal, $y_l(t)$, can be expressed as

$$y_l(t) = \sqrt{2C_l} d_l\left(t - \tau_{0,l}\right) c_l\left(t - \tau_{0,l}\right) \cos\left(2\pi(f_{RF} + f_{d,l})t + \varphi_{0,l}\right), \tag{2}$$

where

- C_l is the power of the lth useful signal;
- $d_l(\cdot)$ is the navigation message;
- $c_l(\cdot)$ is the lth pseudo-random sequence extracted from a family of quasi-orthogonal codes and used for spreading the signal spectrum;

- $\tau_{0,l}$, $f_{d,l}$ and $\varphi_{0,l}$ are the delay, Doppler frequency and phase introduced by the communication channel;
- f_{RF} is the centre frequency of the GNSS signal.

In (1), $i(t)$ can assume different forms depending on the type of interference source. For example, DME and pulsed pseudolite signals are characterized by quite different modulations. Despite such differences, $i(t)$ can, in general, be modeled as

$$i(t) = i_c(t)p_s(t), \tag{3}$$

which is the product of two terms: $i_c(t)$ is a continuous component and $p_s(t)$ is a binary signal assuming values in $\{0, 1\}$ and defining a pulsing sequence. The signal $p_s(t)$ defines the time instants when the interfering signal is effectively transmitted. When pseudolites are considered, $i_c(t)$ assumes the same form as (2).

Furthermore, the duty cycle

$$d = \lim_{T\to+\infty} \frac{1}{T} \int_{-T/2}^{T/2} p_s(t)dt \tag{4}$$

defines the average time during which the pulsed interference is on.

Due to the quasi-orthogonality of the spreading codes, a GNSS receiver is able to process the L useful signals independently and (2) can be simplified to

$$r(t) = y(t) + i_c(t)p_s(t) + \eta(t), \tag{5}$$

where the index, l, has been dropped for ease of notation.

The signal (5) is filtered and down-converted by the receiver front-end before being digitized. Digitization implies two different operations: sampling and amplitude quantization. In the following, sampling and quantization are considered separately. In addition, it is assumed that the signal is sampled without introducing significant distortions. After down-conversion and sampling, (5) becomes:

$$\begin{aligned} r_{IF}[n] &= y_{IF}(nT_s) + i_{c,IF}(nT_s)p_s(nT_s) + \eta_{IF}(nT_s) \\ &= y_{IF}[n] + i_{c,IF}[n]p_s[n] + \eta_{IF}[n], \end{aligned} \tag{6}$$

where the notation $x[n]$ is used to denote a discrete time sequence sampled at the frequency $f_s = \frac{1}{T_s}$. The index "IF" is used to denote a signal down-converted to an intermediate frequency, f_{IF}. In (6), $y_{IF}[n]$ is defined as

$$y_{IF}[n] = \sqrt{2C}d\left(nT_s - \tau_0\right)c\left(nT_s - \tau_0\right)\cos\left(2\pi\left(f_{IF} + f_0\right)nT_s + \varphi_0\right). \tag{7}$$

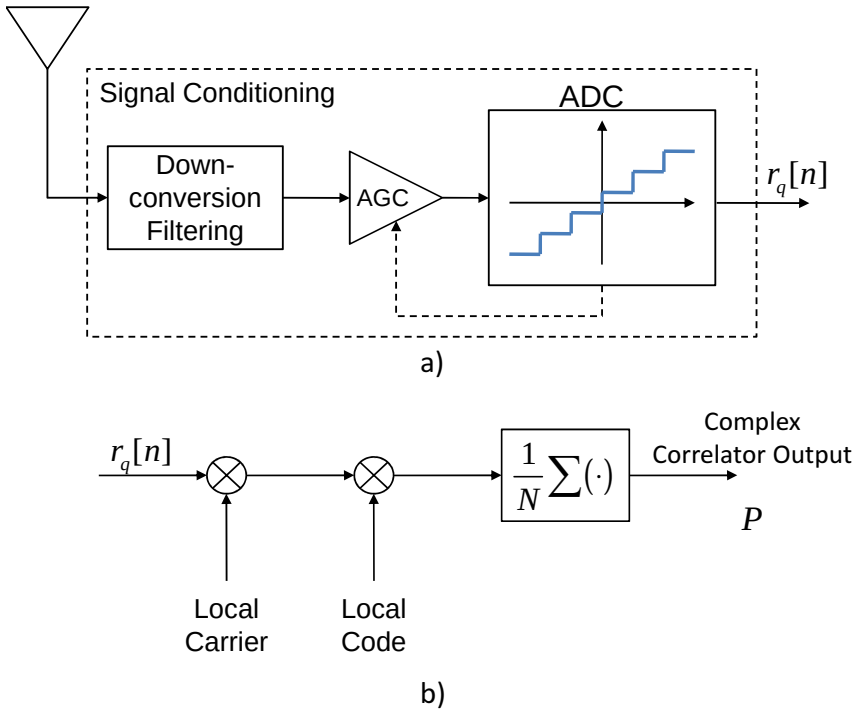

Fig. 1. Basic operations performed by a GNSS receiver. a) Signal conditioning: the RF analog signal is converted into an IF digital sequence. b) The correlation process.

The noise term, $\eta_{IF}[n]$, is assumed to be an Additive White Gaussian Noise (AWGN) with variance σ^2_{IF}. This variance depends on the filtering, down-conversion and sampling strategy applied by the receiver front-end and is given by $\sigma^2_{IF} = N_0 B_{IF}$, where B_{IF} is the front-end one-sided bandwidth and N_0 is the power spectral density of the input noise, $\eta(t)$. The ratio between the carrier power, C, and the noise power spectral density, N_0, defines the Carrier-to-Noise density power ratio (C/N_0), one of the main signal quality indicators used in GNSS.

The amplitude quantization process is shown in the upper part of Fig. 1 and consists of a scaling, introduced by the AGC, and a mapping of the continuous values of $y_{IF}[n]$ into a finite discrete alphabet. This second operation is performed by the ADC. In this paper, ideal and very slow AGCs are considered. Definitions of different AGC types are provided by [17] and the cases considered are characterized by constant AGC gains. An ideal AGC ignores the interference pulse and provides a gain independent from the interference power. In the very slow case, the interference power impacts the selection of the gain, which is fixed according to the

total power measured by the AGC.

Under these conditions, the signal at the output of the ADC can be modeled as:

$$r_q[n] = Q_B\left[A_g\left(y_{IF}[n] + i_{c,IF}[n]p_s[n] + \eta_{IF}[n]\right)\right], \tag{8}$$

where $Q_B(\cdot)$ is the quantization function adopted by an ADC employing B bits for the signal representation. In a uniform quantizer, $Q_B(\cdot)$ is a symmetric stair-case function producing output values in the set $\left\{-2^B+1, -2^B+3, ..., -1, 1, ..., 2^B-3, 2^B-1\right\}$. The parameter A_g is the AGC gain. It is noted that depending on the number of levels used by the ADC and the interference power, several simplifications can be applied to (8). More specifically, two regimes can be considered [19]:

- **small signal mode**: the power of the interference signal is small compared to the noise variance. This allows one to develop a linear approximation of the quantization function $Q_B(\cdot)$. The function $Q_B(\cdot)$ scales the signal components and introduces additional quantization noise;
- **saturation mode**: the interference signal is so powerful that it saturates the receiver ADC. Saturation implies that the pulsed interference, $i_{c,IF}[n]p_s[n]$, is always represented using the highest and lowest levels of the ADC, $\pm A_{max} = \pm 2^B - 1$.

Using the results derived in [19] and [23], it is possible to show that, under the small signal regime, (8) can be approximated as

$$r_q[n] \approx \frac{a_1}{\sigma_{IF}}\left[y_{IF}[n] + i_{c,IF}[n]p_s[n]\right] + \eta_q[n], \tag{9}$$

where $\eta_q[n]$ is a zero mean random variable with variance

$$\text{Var}\left\{\eta_q[n]\right\} = 1 + 8\sum_{i=0}^{2^{B-1}-1} i\text{erfc}\left(\frac{i}{\sqrt{2}A_g\sigma_{IF}}\right), \tag{10}$$

where $\text{erfc}(\cdot)$ denotes the complementary error function [24] and a_1 is a constant given by [23]:

$$a_1 = \sqrt{\frac{2}{\pi}}\left[1 + 2\sum_{i=1}^{2^{B-1}-1}\exp\left\{-\frac{i^2}{2A_g^2\sigma_{IF}^2}\right\}\right]. \tag{11}$$

The term $\eta_q[n]$ is not Gaussian since it also accounts for the additional quantization noise. However, for large values of B, the probability distribution of $\eta_q[n]$ can be approximated by a Gaussian probability density function (pdf).

Under the saturation mode, (8) becomes [19]:

$$r_q[n] \approx Q_B\left[A_g(y_{IF}[n] + \eta_{IF}[n])\right](1 - p_s[n]) + A_{max}\text{sign}\left(i_{c,IF}[n]\right)p_s[n], \tag{12}$$

where sign$(\cdot)$ is the sign function. In this case, the quantization function is applied only to the signal and noise components. An approximation similar to that adopted for the small signal regime can then be applied to the quantized term in (12).

Noticeably, there exists a transition regime modeling the passage between small signal and saturation modes. For such a regime, it is not possible to further simplify (8). In the following, (12) will be used as a basis for the theoretical analysis. It is noted that under the small signal mode, it is possible to use the results derived in [20], where the impact of quantization was neglected and a Gaussian noise term was assumed in (9). For this reason, the small signal case is not considered further in this paper.

After signal conditioning, the sequence $r_q[n]$ is correlated with local replicas of the signal code and carrier. This process is shown in the lower part of Fig. 1 and a complex correlator output is computed as

$$P = \frac{1}{N}\sum_{n=0}^{N-1} r_q[n]c\left(nT_s - \tau\right)\exp\left\{-j2\pi(f_{IF} + f_d)nT_s - j\varphi\right\}, \tag{13}$$

where τ, f_d and φ are the code delay, the Doppler frequency and the phase tested by the receiver. N is the number of samples used for computing a correlator output and $T_c = NT_s$ is the coherent integration time. The computation of correlator outputs is essential for the proper functioning of a GNSS receiver and they are both used in acquisition and tracking [25], which are the main receiver operating modes. Thus, the quality of a GNSS signal can be defined after correlation as [26], [27]:

$$SNR_{out} = \max_{\tau, f_d, \varphi} \frac{|\text{E}\left\{P\right\}|^2}{\frac{1}{2}\text{Var}\left\{P\right\}}, \tag{14}$$

where SNR_{out} is the coherent output SNR. The factor $1/2$ in (14) accounts for the fact that P is a complex quantity and only the variance of its real part is considered.

The loss experienced at the correlator output, due to the presence of interference and after using mitigation techniques, is determined as the ratio between the measured SNR and the ideal coherent output SNR determined under ideal conditions.

III. PULSE BLANKING

In this section, PB is briefly reviewed and its optimality, under specific operating conditions, is discussed.

PB is a pre-correlation mitigation technique, i.e., it is applied to the signal $r_q[n]$ before the correlation process described in Section II. The disturbing signal is removed from $r_q[n]$ by zeroing the samples corrupted by the interference pulses. To achieve this, it is necessary to determine the pulse position, i.e., recover the pulsing scheme, $p_s[n]$. This can be achieved using different estimation techniques as discussed below.

When the pulsing scheme, $p_s[n]$, is known and the saturation regime is considered, PB becomes the optimal mitigation technique in the Maximum Likelihood (ML) sense. More specifically, two types of random variables can be identified in (12):

- signal and noise samples, $Q_B\left(A_g(y_{IF}[n]+\eta_{IF}[n]\right)$, characterized by the probability mass function (pmf) $f_y\left(y|y_{IF}[n],\sigma_{IF}^2\right)$,
- interference samples, $A_{max}\text{sign}\left(i_{c,IF}[n]\right)$, characterized by the pmf $f_i\left(i|i_{c,IF}[n]\right)$.

The pmf $f_y\left(y|y_{IF}[n],\sigma_{IF}^2\right)$ can have a complex expression and is a function of the useful signal samples and its parameters. The function $f_i\left(i|i_{c,IF}[n]\right)$ is a scaled Bernoulli pmf with mean depending on $i_{c,IF}[n]$. Moreover, due to ADC saturation, $f_i\left(i|i_{c,IF}[n]\right)$ is independent of the useful signal, $y_{IF}[n]$. If all the samples of $r_q[n]$ are assumed statistically independent, then the associated log-likelihood function can be written as

$$\log\left(L_{sat}\left(\tau,f_d,\varphi\right)\right)=\sum_{n=0,p_s[n]=0}^{N-1}\log\left[f_y\left(y|y_{IF}[n],\sigma_{IF}^2\right)\right]+\sum_{n=0,p_s[n]=1}^{N-1}\log\left[f_i\left(i|i_{c,IF}[n]\right)\right] \quad (15)$$

where the position of the pulse is assumed known. In order to determine the signal parameter estimates, $\{\tau,f_d,\varphi\}$, the derivative of (15) has to be computed. Since the second summation in (15) is independent of $\{\tau,f_d,\varphi\}$, the derivative of this part of the likelihood is zero. This implies that the ML estimator of $\{\tau_0,f_{d,0},\varphi_0\}$ is independent of the interference samples that have to be excised. This operation is performed by pulse blanker which zeros the interference samples $A_{max}\text{sign}\left(i_{c,IF}[n]\right)$. PB is thus the optimal mitigation technique, in the ML sense, in the presence of ADC saturation.

Eq. (15) has been computed assuming the knowledge of the pulsing scheme, $p_s[n]$. This condition is rarely verified and an estimation block is required to determine $p_s[n]$. Several

methods are available in the literature for determining the pulse position. In the following section, two cases are considered:

- **ideal blanking**: the pulse position is assumed known by the receiver. This could be the case of a participating pseudolite receiver, which continuously tracks pseudolite signals using a correlation-based process.
- **thresholding**: the pulse position is detected by comparing the input samples with a decision threshold, T. If $|r[n]|$ is greater than T, then the interference is declared present. Thus, pulse positions are determined through threshold passing.

IV. PB SNR Loss in the Presence of Signal Conditioning

A theoretical model for the loss associated with pulse blanking in the presence of quantization is provided in this section. In order to simplify the analysis, it is assumed that pulsed interference is saturating the ADC. For this case no results seem to be available in the literature, whereas the loss experienced under the small signal regime can be obtained using the findings of [20].

Before providing the loss model for PB using thresholding, some issues should be considered:

- if pulse positions were perfectly known, then pulsed interference would always be removed and the loss is given by the product of two terms: the quantization loss and the excision loss. The quantization loss is given by [28]:

$$L_q = \frac{2}{\pi} \frac{\left[1 + 2\sum_{i=1}^{2^{B-1}-1} \exp\left\{-\frac{i^2}{2A_g^2\sigma_{IF}^2}\right\}\right]^2}{1 + 8\sum_{i=1}^{2^{B-1}-1} i\text{erfc}\left(\frac{i}{\sqrt{2}A_g\sigma_{IF}}\right)}, \tag{16}$$

  whereas the excision loss is equal to

$$L_{ex} = 1 - d \tag{17}$$

  and corresponds to an effective reduction in the integration time since dN samples are removed by blanking. The loss under ideal pulse synchronization conditions is thus given by

$$L_{ib} = L_q \cdot L_{ex}. \tag{18}$$

- when a single bit is used for quantization, it is not possible to determine the pulse position using a decision threshold. All the input samples are characterized by the same magnitude and, thus, is not possible to discriminate between useful and interfering signals;

- when PB is not implemented, the degradation due to pulsed interference corresponds to the saturation loss derived by [19]. It has been shown that receivers using a low number of bits have a natural immunity against pulsed interference. Thus, the saturation loss derived by [19] is used here as a comparison term;
- since PB is applied after quantization and the ADC produces values in the set

$$\left\{-2^B+1, -2^B+3, ..., -1, 1, ..., 2^B-3, 2^B-1\right\},$$

the decision threshold, T, can assume only a limited number of values. Setting a threshold higher than $A_{max} = 2^B - 1$ is equivalent to disabling blanking, whereas having a threshold lower than 1 causes the excision of all the samples. In addition to this, thresholds with values between the same subsequent ADC output levels lead to the same pulse detection. For this reason, only thresholds in the set $\left\{2, 4, ..., 2^{B-1}\right\}$ are considered.

As for the ideal pulse synchronization case (denoted in the following as ideal blanking), the loss experienced when using thresholding can be expressed as the product of two terms:

$$L_{pb} = L_T \cdot L_{ex}, \tag{19}$$

where L_T is the quantization loss experienced in the presence of thresholding. It must be remarked that this decomposition is only valid when the interference pulse is saturating the receiver ADC. Since the blanking threshold has to be lower than the maximum ADC level and the interference is saturating the receiver ADC, then it is possible to assume that the interference pulse is always removed. This assumption will be further discussed in Section V where experimental results are presented.

The loss, L_T, is derived by using an approach similar to that adopted by [28] for computing the quantization loss in the absence of pulse blanking. Using (6), the quantizer input can be expressed as

$$r_q[n] = A_g(y[n] + \eta_{IF}[n]), \tag{20}$$

where $y[n] = y_{IF}[n] + i_{c,IF}[n]p_s[n]$ denotes the non-zero mean terms in (6). From (20), it is possible to determine the probability that the quantized signal, $r_q[n]$, assumes the value $2i+1$

when B bits are used for signal quantization

$$p_{B,2i+1} = P\left(r_q[n] = 2i+1\right)$$
$$= \begin{cases} \frac{1}{\sqrt{2\pi\sigma_{IF}^2}} \int_{i/A_g - y[n]}^{+\infty} \exp\left\{-\frac{z^2}{2\sigma_{IF}^2}\right\} dz & \text{for } i = 2^{B-1}-1 \\ \frac{1}{\sqrt{2\pi\sigma_{IF}^2}} \int_{-\infty}^{(i+1)/A_g - y[n]} \exp\left\{-\frac{z^2}{2\sigma_{IF}^2}\right\} dz & \text{for } i = -2^{B-1} \\ \frac{1}{\sqrt{2\pi\sigma_{IF}^2}} \int_{i/A_g - y[n]}^{(i+1)/A_g - y[n]} \exp\left\{-\frac{z^2}{2\sigma_{IF}^2}\right\} dz & \text{otherwise.} \end{cases} \tag{21}$$

The first two lines in (21) correspond to the probability that $r_q[n]$ is equal to the highest/lowest values of the quantizer output. Thus, the integrals are extended to include the tails of the input noise distribution. In the following, it is assumed that at least the highest and lowest values of $r_q[n]$ are removed when blanking is used. Thus, the first and second moments of $r_q[n]$ can be computed as:

$$E[r_q[n]] = \sum_{i=0}^{K} (2i+1)\left[p_{B,2i+1} - p_{B,-(2i+1)}\right] \tag{22}$$

and

$$E[r_q^2[n]] = \sum_{i=0}^{K} (2i+1)^2\left[p_{B,2i+1} + p_{B,-(2i+1)}\right], \tag{23}$$

where

$$K = \left\lfloor \frac{T-1}{2} \right\rfloor \tag{24}$$

is the number of positive levels not clipped by the blanker. Assuming that the magnitude of the useful signal is small compared to the noise standard deviation, it is possible to approximate the probability difference in (22) as

$$p_{B,2i+1} - p_{B,-2(2i+1)} \approx \frac{2y[n]}{\sqrt{2\pi\sigma_{IF}^2}} \left[\exp\left\{-\frac{i^2}{2A_g^2\sigma_{IF}^2}\right\} - \exp\left\{-\frac{(i+1)^2}{2A_g^2\sigma_{IF}^2}\right\}\right]. \tag{25}$$

The assumption of small signal amplitude can be considered valid even in the presence of interference since strong pulses are removed through blanking. Blanking is implicitely accounted for in the summation limits in (22) and (23).

Approximation (25) is based on the geometric interpretation provided in Fig. 2. The probability difference reduces to the difference of the areas of the two narrow stripes depicted in the bottom part of Fig. 2. Each area is then approximated by that of the rectangle having $2y[n]$ as base and $\frac{1}{\sqrt{2\pi\sigma_{IF}^2}} \exp\left\{-\frac{x^2}{2A_g^2\sigma_{IF}^2}\right\}$ as height. For the two stripes $x = i$ and $x = i+1$ are applied respectively. It is noted that the approximation in (25) is not valid for the values of i corresponding

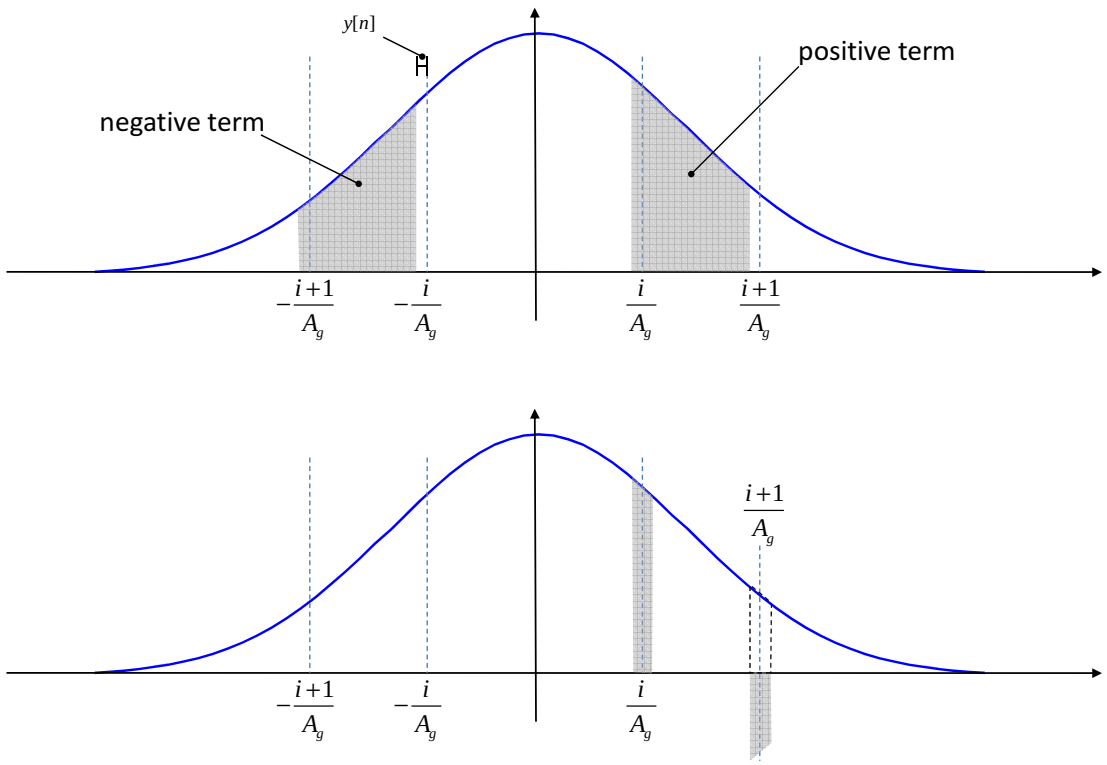

Fig. 2. Geometric interpretation of the probability difference defined by (25).

to the highest/lowest quantization levels. However, those values are discarded since they will be eliminated by the blanker.

Using (25), the first moment (22) becomes

$$\begin{aligned} E[r_q[n]] &= \frac{2y[n]}{\sqrt{2\pi\sigma_{IF}^2}} \sum_{i=0}^{K} (2i+1) \left[\exp\left\{ -\frac{i^2}{2A_g^2\sigma_{IF}^2} \right\} - \exp\left\{ -\frac{(i+1)^2}{2A_g^2\sigma^2} \right\} \right] \\ &= \frac{2y[n]}{\sqrt{2\pi\sigma_{IF}^2}} \left[1 + 2\sum_{i=1}^{K} \exp\left\{ -\frac{i^2}{2A_g^2\sigma_{IF}^2} \right\} - (2K+1) \exp\left\{ -\frac{(K+1)^2}{2A_g^2\sigma_{IF}^2} \right\} \right] \\ &= \frac{a_2}{\sqrt{\sigma_{IF}^2}} y[n], \end{aligned} \tag{26}$$

where

$$a_2 = \sqrt{\frac{2}{\pi}} \left[1 + 2\sum_{i=1}^{K} \exp\left\{ -\frac{i^2}{2A_g^2\sigma_{IF}^2} \right\} - (2K+1) \exp\left\{ -\frac{(K+1)^2}{2A_g^2\sigma_{IF}^2} \right\} \right]. \tag{27}$$

The second moment can be computed by approximating the probability sum in (23) as

$$p_{B,2i+1} + p_{B,-2(2i+1)} \approx \text{erfc}\left(\frac{i}{\sqrt{2}A_g\sigma_{IF}} \right) - \text{erfc}\left(\frac{i+1}{\sqrt{2}A_g\sigma_{IF}} \right). \tag{28}$$

This approximation is based on the approach adopted by [28] and exploits the fact that $\frac{|y[n]|}{\sigma_{IF}} \ll 1$.

Using (28), the second moment in (23) becomes

$$\begin{aligned} E[r_q^2[n]] &= \sum_{i=0}^{K}(2i+1)^2\left[\text{erfc}\left(\frac{i}{\sqrt{2}A_g\sigma_{IF}}\right) - \text{erfc}\left(\frac{i+1}{\sqrt{2}A_g\sigma_{IF}}\right)\right] \\ &= 1 + 8\sum_{i=1}^{K} i\text{erfc}\left(\frac{i}{\sqrt{2}A_g\sigma_{IF}}\right) - (2K+1)^2\text{erfc}\left(\frac{K+1}{\sqrt{2}A_g\sigma_{IF}}\right). \end{aligned} \tag{29}$$

Finally, by following the same approach adopted in [28], it is possible to show that the loss due to blanking and quantization is given by

$$L_T = \frac{a_2^2}{E[r_q^2[n]]} = \frac{2}{\pi}\frac{\left[1 + 2\sum_{i=1}^{K}\exp\left\{-\frac{i^2}{2A_g^2\sigma_{IF}^2}\right\} - (2K+1)\exp\left\{-\frac{(K+1)^2}{2A_g^2\sigma_{IF}^2}\right\}\right]^2}{1 + 8\sum_{i=1}^{K} i\text{erfc}\left(\frac{i}{\sqrt{2}A_g\sigma_{IF}}\right) - (2K+1)^2\text{erfc}\left(\frac{K+1}{\sqrt{2}A_g\sigma_{IF}}\right)}. \tag{30}$$

Note that in most of the previous literature [1], [2], [7], the impact of the thresholding loss, L_T, has been neglected and the sole excision loss (17) has been adopted to quantify the degradation introduced by PB. This approximation is valid only when a large number of bits, B, is available for signal quantization. More specifically, it is possible to show that (30) converges to 1 for large values of B and K. The proposed loss model allows one to quantify the SNR degradation even when few bits are available for the signal representation.

The thresholding loss, L_T, is depicted in Fig. 3 as a function of the normalized AGC gain, $A_g\sigma_{IF}$, for the case of a 3 bit quantizer. The quantization loss (16) has also been provided for comparison purposes.

From (30) and Fig. 3, it is possible to conclude that the optimal blanker threshold, T, is given by

$$T_{opt} = 2^B - 2 \tag{31}$$

i.e., only the samples equal to $\pm A_{max}$ are removed. This implies that only two levels of the quantization function, Q_B, are used for pulse detection, whereas all the other levels are used for the useful signal representation.

The optimal AGC level is also lower than that obtained in the absence of interference. This result is explained by the fact that the useful signal and noise should be represented without using the highest/lowest levels of the quantization function. For AGC gain values close to the optimum, L_T is close to L_q, where L_q is the quantization loss. The optimal AGC gains when $T = 2^B - 2$ are provided in Table I as a function of the number of bits, B.

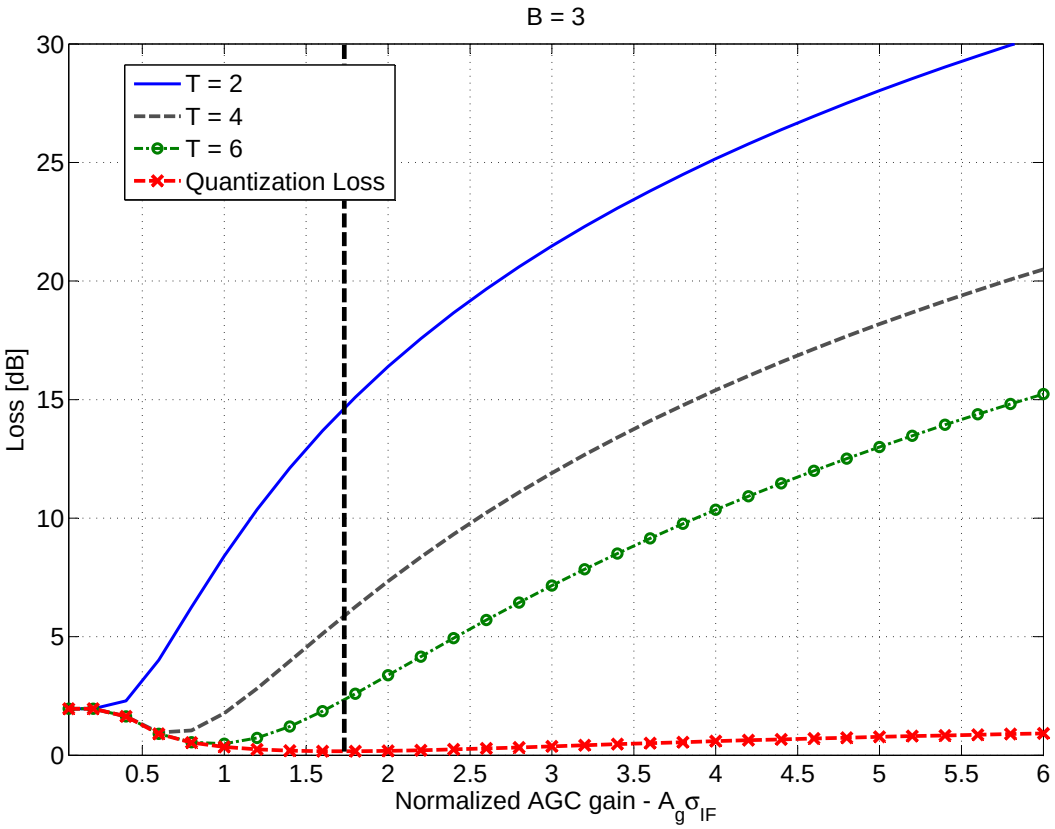

Fig. 3. Thresholding loss, L_T, for a 3 bit quantizer as a function of the normalized AGC gain, $A_g\sigma_{IF}$. The vertical line indicates the optimal AGC gain in the absence of interference.

TABLE I

OPTIMAL AGC GAINS IN THE PRESENCE OF PULSE BLANKING FOR $T = 2^B - 1$

No. of Bits	Normalized AGC gain, $A_g\sigma_{IF}$	Loss [dB]
2	0.2	1.96 dB
3	0.936	0.47 dB
4	1.888	0.115 dB
5	3.64	0.03 dB
6	6.95	0.008 dB

The properties of the composite loss (19) are further analyzed in Fig. 4, where a duty cycle equal to 10% is considered. Four cases are analyzed: "Optimal Thresholding" refers to the case where L_T is computed for $T = T_{opt}$, the "No Blanking" curve has been obtained without applying any mitigation technique and "Ideal Blanking" corresponds to (18). The "No Blanking" case has been obtained using the saturation model proposed by [19]. Finally, the "Excision Loss" curve refers to the sole excision loss (17) adopted by [7] to quantify the impact of PB.

From Fig. 4 it can be observed that PB with thresholding is effective only if the AGC gain is properly set. In that case, the performance of thresholding is close to that achieved when the pulse position is known. It is also noted that the "Optimal Thresholding" and "No Blanking" curves have an intersection point. For an AGC gain greater than the intersection point, PB becomes ineffective and introduces additional signal losses. The "Excision Loss" curve consistently underestimates the loss introduced by PB and does not depend on the AGC/ADC parameters. Differences between the proposed loss model ("Optimal Thresholding") and the excision loss [7] clearly appear for $B = 2$ and $B = 3$. For $B = 4$, the models which consider the effects of PB converge to the sole excision loss when the normalized AGC gain is properly selected. The equivalence of the different models becomes more evident for larger values of B. These results are supported by simulations and measurements in Section V. From the analysis, the ability of the proposed model to predict the loss introduced by PB as function of the AGC/ADC parameters clearly emerges. Previous models [1], [2], [7] are unable to capture the interaction of the pulse blanker with receiver AGC/ADC.

V. Simulation and Experimental Results

In this section, simulation and experimental results supporting the theoretical model developed for the computation of the SNR loss are provided when PB is applied. Note that simulations and experimental analysis have complementary characteristics. The former allows one to obtain statistically significant results in a controlled environment. The latter shows that the theory developed has a direct impact on the design of real systems/devices and demonstrates the relevance of the obtained results. For this reason, simulations and real data analysis are adopted in this paper.

For the simulation analysis, Global Positioning System (GPS) L1 signals corrupted by a pulsed pseudolite component were generated and used for the evaluation of the SNR loss. The pseudolite

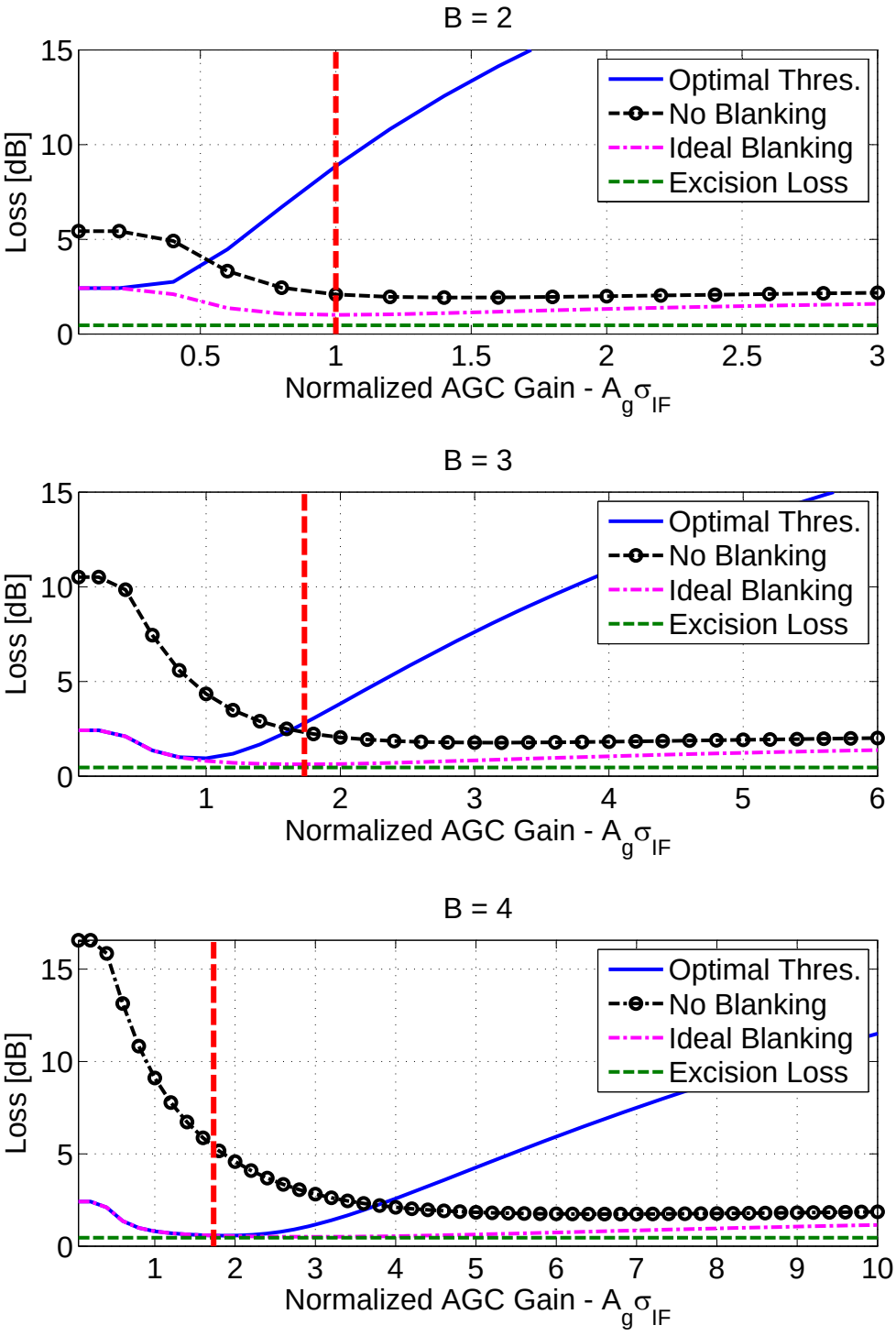

Fig. 4. Comparison of the SNR losses that a GNSS receiver would experience in the presence of pulsed interference for different number of bits and AGC gains. Vertical lines indicate the optimal AGC gain in the absence of interference. Pulse duty cycle, $d = 10\%$

TABLE II

PARAMETERS USED FOR THE EVALUATION OF A PB MITIGATION TECHNIQUE THROUGH SIMULATIONS.

Parameter	Value
Coherent integration time, T_c	1 ms
Sampling frequency, f_s	5 MHz
Intermediate frequency, f_{IF}	1.42 MHz
C/N_0 of the GPS L1 system	45 dB-Hz
Number of Monte Carlo Simulation runs	10^5

component was characterized by a modulation similar to that of GPS Coarse/Acquisition (C/A) signals. The generated signal was processed using a GNSS software receiver able to estimate the C/N_0 from the correlator outputs. The SNR loss is computed as the difference between the input C/N_0, used for the simulation of the useful GPS signals, and the C/N_0 estimated in the presence of pulsed interference. The main parameters used for the simulation analysis are provided in Table II.

Sample simulation results are shown in Fig. 5, where the SNR loss is depicted as a function of the normalized AGC gain and for different values of the threshold T. In this particular example, $B = 4$ and $d = 0.1$ were considered. Simulation results are in good agreement with the theoretical findings, supporting the validity of the theoretical framework developed for quantifying the loss in the presence of pulsed interference and PB.

The second part of this section is devoted to the analysis of experimental results obtained using the setup depicted in the upper part of Fig. 6. A Spirent GSS8000 hardware simulator was used to generate a constellation of GPS satellites broadcasting L1 signals in an anechoic chamber. The PL interfering signal was generated by an USRP2 device, which was placed in the anechoic chamber as illustrated in Fig. 6. The software interface developed for controlling the parameters of the USRP2 pseudolite is depicted in the bottom part of Fig. 6. Experimental data were collected using a NI PXI-e 5663 signal vector analyzer with a 14-bit ADC. A dataset was collected in the absence of pseudolite signal and used as a baseline for the computation of the SNR loss. Experimental data were then post-processed and a re-quantization module was developed to mimic the effect of an ADC operating with a limited number of bits. The re-quantization module implements AGC scaling and ADC mapping. The case of an ideal AGC,

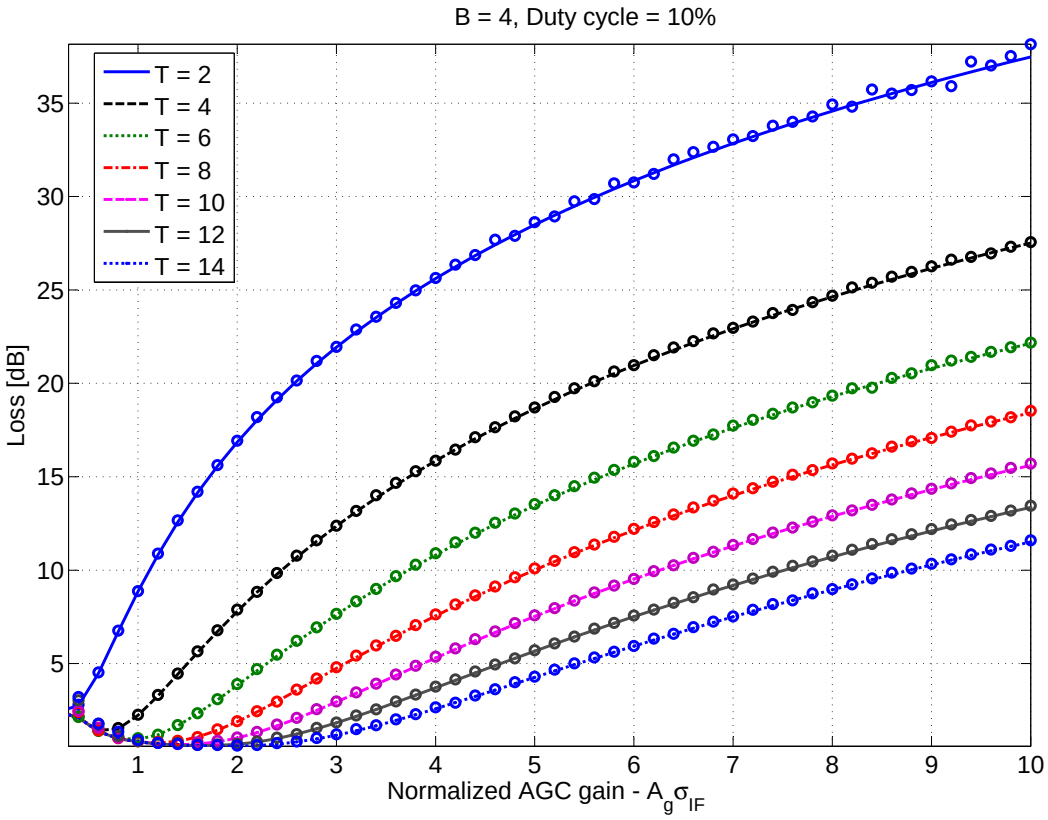

Fig. 5. Comparison between Monte Carlo and theoretical results. Circles are used to indicate simulation results.

able to ignore the presence of pulsed interference, was considered. In this respect, the input noise variance, σ_{IF}^2, was determined using a robust noise variance estimator [21]. More specifically, the noise variance is estimated considering data blocks of 0.1 ms duration. Several (ten for the experiments detailed in the following) estimates are then stored in memory and the final variance is obtained as the median of the stored values:

$$\sigma_{IF}^2 = \text{MED}\left(\hat{\sigma}_0^2, \hat{\sigma}_1^2, ..., \hat{\sigma}_{P-1}^2\right). \tag{32}$$

In (32), $\{\hat{\sigma}_0^2\}_{i=0}^{P-1}$ are the sample variances computed using subsequent 0.1 ms blocks of data. The symbol "MED" is used to denote the median operation [21] which is robust against outliers and it is used to discard abnormal variance estimates obtained in the presence of interference pulses. The effectiveness of (32) has been empirically verified and its detailed analysis is out of the scope of this paper. Finally, the AGC gain was set according to the optimal values provided in Table I.

The re-quantization module described above was used to obtain datasets with samples that are quantized using different numbers of bits. The data obtained were finally processed using a GPS software receiver implementing PB. The software receiver was employed to estimate the signal C/N_0 and empirically determine the impact of PB.

In Fig. 7, the different stages used for the processing of the un-quantized GNSS signal are shown. In the upper part of Fig. 7, the un-quantized signal after AGC scaling is shown. The signal was recovered using a 5 MHz sampling frequency and complex In-phase/Quadrature (I/Q) sampling [29] was implemented by the NI front-end. The pseudolite signal component clearly emerges from the recovered samples; moreover a low frequency modulation can be observed on the pseudolite pulses. This is due to the clock drifts of the USRP2 and NI platforms. The I/Q signal components are quantized independently by the ADC and the pseudolite pulses are clipped to the maximum amplitude representable by the ADC. The quantized signal before PB is shown in the central plot of Fig. 7. Finally, PB is implemented and the result is shown in the bottom part of Fig. 7. In this case, a sample is blanked if either its real or imaginary part passes the threshold, T. The blanking threshold has been set according to the criteria discussed in Section IV. Note that the AGC has properly scaled the useful input samples that are not affected by blanking. From Fig. 7, it emerges that some residual pulse samples are not excised by the blanker. These samples do not saturate the ADC and are caused by sign transitions and oscillations due to the transmitter and receiver clock drifts. Most of the PL signal samples are, however, removed and the remaining components have small amplitudes. Their effect is thus negligible.

Signals processed according to the aforementioned procedure have been used to assess empirically the impact of PB. Sample results in terms of estimated C/N_0 are provided in Fig. 8, where the 3 bit case is considered. From the figure, it emerges that PB allows one to achieve performance close to that obtained in the absence of interference. More specifically, the average difference between the C/N_0 estimated in the absence of interference and the one determined after PB is approximately 0.9 dB. This result is in agreement with the theoretical findings provided in Section IV. The C/N_0 estimated after quantization and without PB is also provided in Fig. 8. Quantization was performed by considering the optimal AGC scaling in the absence of interference. The advantages of PB clearly emerge: PB is an effective interference mitigation technique even when a limited number of bits are available for the signal representation. In this

case, PB provides a C/N_0 gain of about 4 dB which is in agreement with the results depicted in Fig. 4. Finally, the C/N_0 estimated from the un-quantized signal is provided. As expected, and in agreement with the theory developed by [23] and [19], the un-quantized signal is the most affected by pulsed interference.

Similar results were obtained considering different satellite signals and number of bits. These results are not provided here in order to avoid the repetition of similar findings.

Monte Carlo simulations and experimental analysis support the validity of the theoretical framework developed in Section IV, which provides effective criteria for the design and implementation of PB techniques even in the presence of a limited number of bits for the signal representation. From the analysis, it emerges that the design of a pulse blanker is not limited to the selection of the blanking threshold but it also requires the careful design of the AGC/ADC response.

VI. Conclusions

In this paper, PB has been analyzed in the presence of quantization and AGC scaling and a novel theoretical framework for determining the SNR loss was suggested. The findings obtained provide useful insights into the process of PB and constitute an effective tool for setting PB parameters. When thresholding is adopted for determining the position of the interference pulse, only the lowest/highest level of the quantization function should be used for pulse detection. The AGC gain should also be reduced, with respect to the case of interference absence, to avoid the excision of useful signal components.

Simulations and real data analysis support the validity of the theoretical framework developed in the paper and show the effectiveness of the criteria derived for the design of PB techniques.

References

[1] C. Hegarty, A. J. V. Dierendonck, D. Bobyn, M. Tran, and J. Grabowski, "Suppression of pulsed interference through blanking," in *Proc. of the IAIN World Congress and the Annual Meeting of The Institute of Navigation AM/ION*, San Diego, CA, jun 2000, pp. 399–408, weak pulse model.

[2] J. Grabowski and C. Hegarty, "Characterization of l5 receiver performance using digital pulse blanking," in *Proc. of the ION GPS*, Portland, OR, sep 2002, pp. 1630–1635.

[3] P. Madhani, P. Axelrad, K. Krumvieda, and J. Thomas, "Application of successive interference cancellation to the GPS pseudolite near-far problem," *IEEE Trans. Aerosp. Electron. Syst.*, vol. 39, no. 2, pp. 481 – 488, Apr. 2003.

[4] M. Paonni, J. Jang, B. Eissfeller, S. Wallner, J. R. J., Samson, and F. Fernandez, "Innovative interference mitigation approaches: Analytical analysis, implementation and validation," in *ESA Workshop on Satellite Navigation Technologies and European Workshop on GNSS Signals and Signal Processing (NAVITEC)*, Dec. 2010, pp. 1 –8.

[5] J. K. Holmes, *Spread Spectrum Systems for GNSS and Wireless Communications*, ser. GNSS Technology and Applications. Artech House, May 2007.

[6] R. Landry, V. Calmettes, and M. Bousquet, "Impact of interference on a generic GPS receiver and assessment of mitigation techniques," in *Proc. of the 5th IEEE International Symposium on Spread Spectrum Techniques and Applications*, vol. 1, Sept. 1998, pp. 87 –91.

[7] T. Pany, *Navigation Signal Processing for GNSS Software Receivers*, ser. GNSS Technology and Applications. Artech House, Jan. 2010.

[8] S. A. Nava and S. Scarafia, "Analysis and simulations of mitigation techniques for pulsed interferers on GNSS signals," Ph.D. dissertation, Politecnico di Torino, sep 2006.

[9] T. Kim and J. Grabowski, "Validation of GPS L5 coexistence with DME/TACAN and link-16 systems," in *Proc. of the 16th International Technical Meeting of the Satellite Division of The Institute of Navigation, ION GPS/GNSS*, Portland, OR, Sept. 2003, pp. 1455 – 1469.

[10] F. Bastide, "Analysis of the feasibility and interests of galileo E5a/E5b and GPS L5 signals for use with civil aviation," PhD Thesis, Institut National Polytechnique de Toulouse, Oct. 2004.

[11] F. Bastide, C. Macabiau, D. Akos, and B. Roturier, "Assessment of L5 receiver performance in presence of interference using a realistic receiver simulator," in *Proc. of the 16th International Technical Meeting of the Satellite Division of The Institute of Navigation, ION GPS/GNSS*, Portland, OR, Sept. 2003, pp. 142–152.

[12] G. X. Gao, "DME/TACAN interference and its mitigation in L5/E5 bands," in *Proc. of the ION/GNSS*, Fort Worth, TX, sep 2007, pp. 1191–1200.

[13] F. Bastide, E. Chatre, C. Macabiau, and B. Roturier, "GPS L5 and galileo E5a/E5b signal-to-noise density ratio degradation due to DME/TACAN signals: Simulations and theoretical derivation," in *Proceedings of the National Technical Meeting of The Institute of Navigation, ION/ITM*, San Diego, CA, Jan. 2004, pp. 1049–1062.

[14] C. O'Driscoll, D. Borio, and J. Fortuny, "Scoping study on pseudolites," Joint Research Centre of the EC, http://publications.jrc.ec.europa.eu/repository/handle/111111111/16264, Technical Report JRC64608, May 2011.

[15] J. Barnes, C. Rizos, J. Wang, D. Small, G. Voigt, and N. Gambale, "Locata: A new positioning technology for high precision indoor and outdoor positioning," in *Proc. of the 16th International Technical Meeting of the Satellite Division of The Institute of Navigation, ION GPS/GNSS*, Portland, OR, Sept. 2003, pp. 1119–1128.

[16] K. R. Zimmerman, H. S. Cobb, F. N. Bauregger, S. Alban, P. Y. Montgomery, and D. G. Lawrence, "A new gps augmentation solution: Terralite xps system for mining applications and initial experience," in *Proc. of the 18th International Technical Meeting of the Satellite Division of The Institute of Navigation, ION GNSS*, Long Beach, CA, Sept. 2005, pp. 2775–2788.

[17] S. H. Cobb, "GPS pseudolites: Theory, design and applications," PhD Thesis, Stanford University, Sept. 1997.

[18] D. Borio and J. Fortuny, "Impact of pseudolite signals on non-participating GPS receivers: Compatibility analysis for commercial receivers," EC Joint Reseach Centre, Tech. Rep., November 2010.

[19] D. Borio, C. O'Driscoll, and J. Fortuny, "Impact of pseudolite signals on non-participating GNSS receivers. modelling receiver losses," EC Joint Reseach Centre, Tech. Rep., October 2011.

[20] F. Soualle, M. Cattenoz, K. Giger, and C. Zecha, "Improved analytical models of SNIR degradation in presence of pulsed signals and impact of code-pulse synchrony," in *Proc. of the Fifth European Workshop on GNSS Signals and Signal*

Processing, Institut Aéronautique et Spatial (IAS), Toulouse, France, Dec. 2011, the impact of quantization is neglected Only limite cases for the threshold are selected (no blanking/'optimal'threholding).

[21] R. A. Maronna, D. R. Martin, and V. J. Yohai, *Robust Statistics: Theory and Methods*, ser. Series in Probability and Statistics. Wiley, May 2006.

[22] D. Borio and E. Cano, "Evaluation of GNSS pulsed interference mitigation techniques accounting for signal conditioning," in *Proc. of the European Navigation Conference (ENC)*, Gdanks, Poland, April 2012, pp. 1–10.

[23] D. Borio, C. O'Driscoll, and J. Fortuny, "Impact of pseudolite signals on non participating GNSS receivers," in *Proc. of the European Navigation Conference*, London, UK, Nov. 2011, pp. 1–11.

[24] M. Abramowitz and I. A. Stegun, *Handbook of Mathematical Functions with Formulas, Graphs, and Mathematical Tables*. New York: Dover, 1964.

[25] E. D. Kaplan and C. Hegarty, Eds., *Understanding GPS: Principles and Applications*, 2nd ed. Artech House Publishers, Nov. 2005.

[26] J. W. Betz, "Effect of partial-band interference on receiver estimation of C/N_0," in *Proc. of the 2001 National Technical Meeting of The Institute of Navigation*, Long Beach, CA, Jan. 2001, pp. 817 – 828.

[27] ——, "Effect of narrowband interference on GPS code tracking accuracy," in *Proc. of ION National Technical Meeting*, Anaheim, CA, Jan. 2000, pp. 16–27.

[28] D. Borio, "A statistical theory for GNSS signal acquisition," PhD Thesis, Politecnico di Torino, Apr. 2008.

[29] J. B.-Y. Tsui, *Fundamentals of GPS Receivers*, 2nd ed. Wiley-Interscience, Dec. 2004.

a)

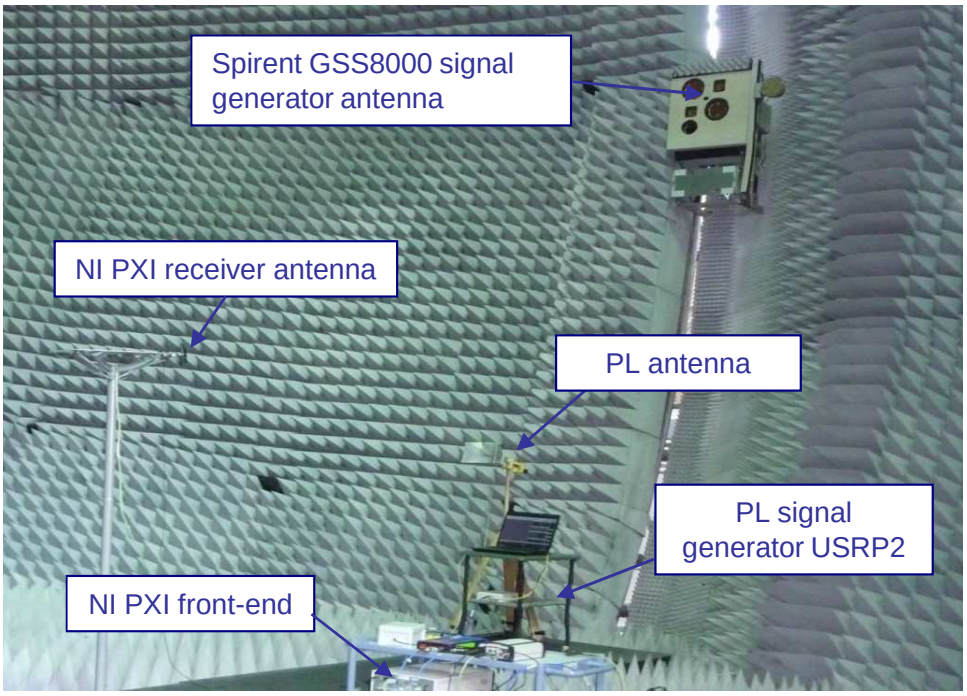

b)

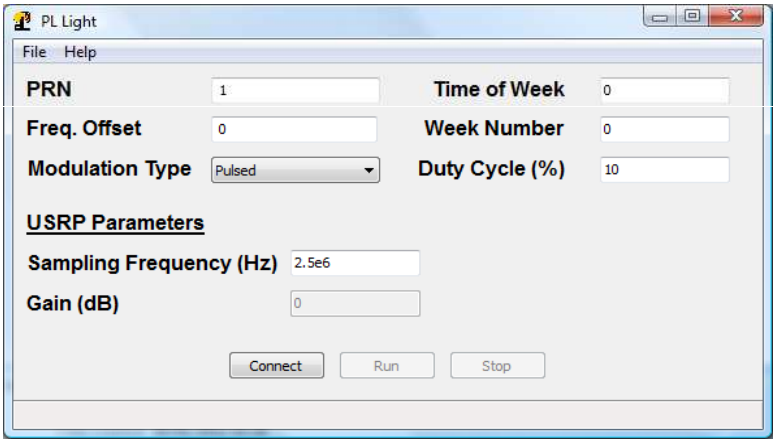

Fig. 6. Experimental setup. a) A snapshot of the anechoic chamber where collection of GPS L1 data impaired by PL pulsed interference is carried out. b) GUI of the PL software tool.

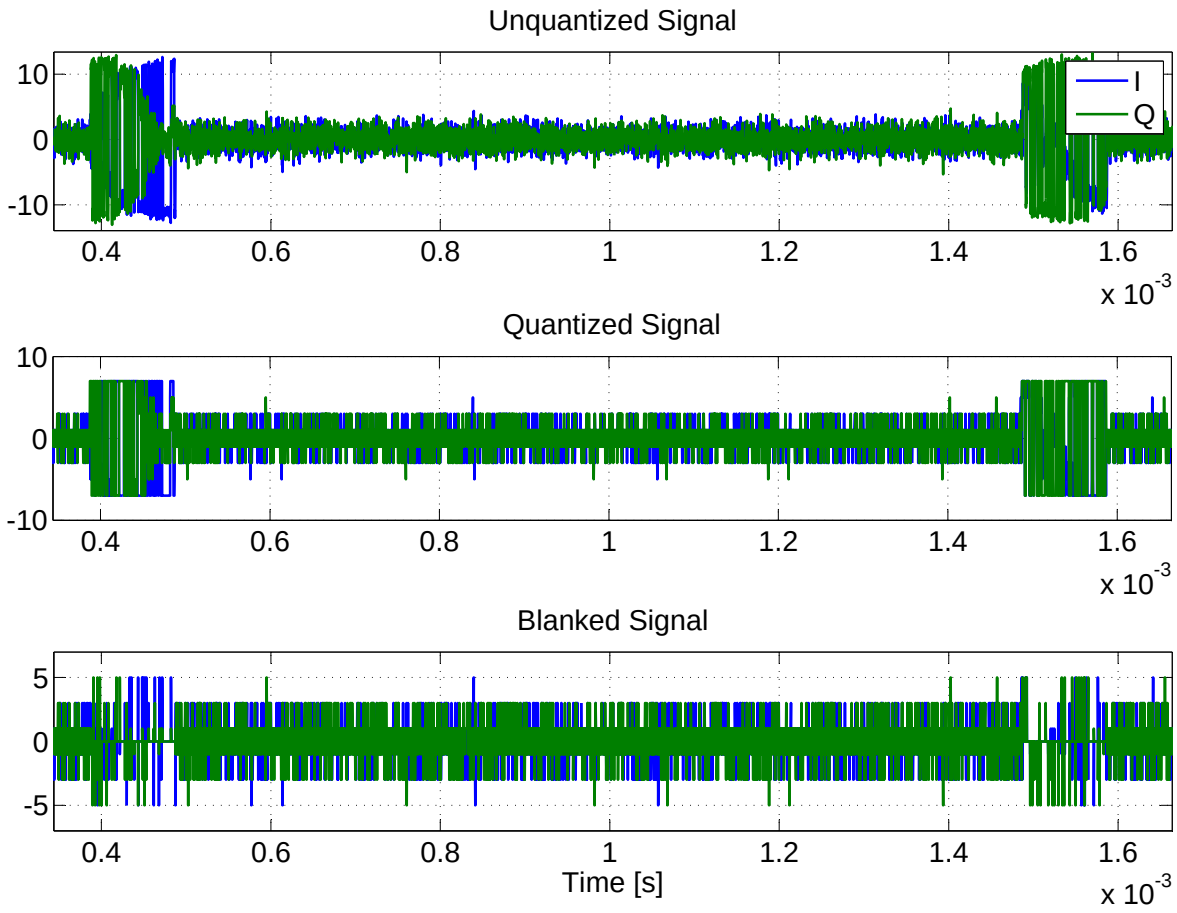

Fig. 7. Different stages used for the processing of signals affected by pulsed interference. The un-quantized signal after AGC scaling is shown in the upper part of the figure. The central plot shows the signal after quantization and, finally, the signal after PB is provided in the bottom part.

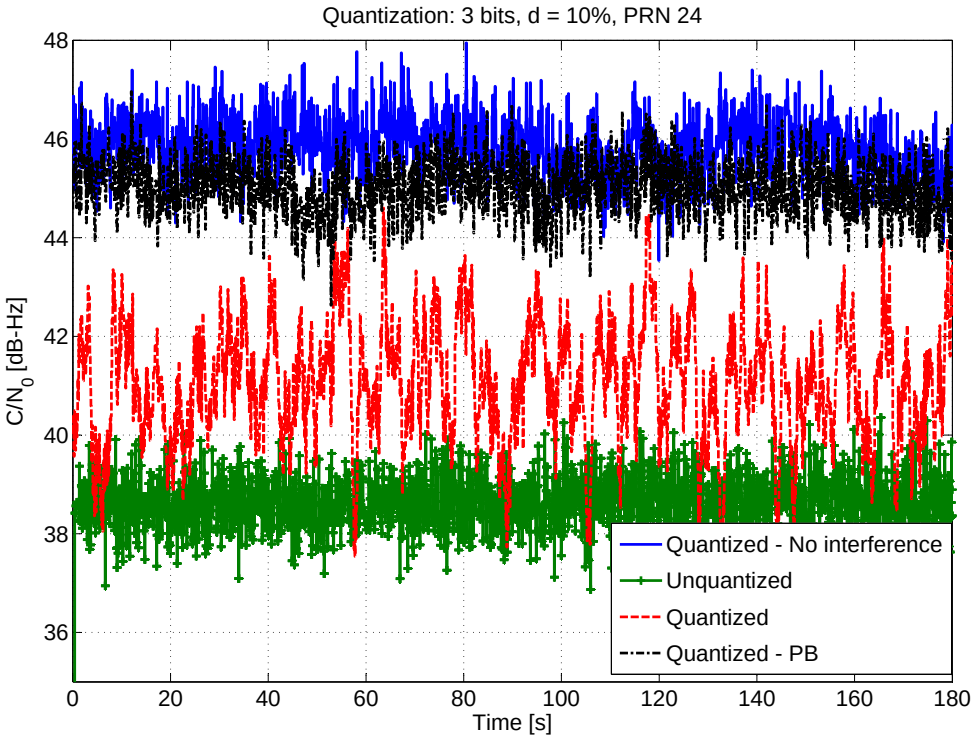

Fig. 8. Comparison of C/N_0 values estimated under different operating conditions. The use of a pulse blanker significantly improves the performance of a GNSS receiver even in the presence of strong quantization. In this case, the signal was re-quantized using 3 bits.